GaSe-assisted microfiber autocorrelator for characterizing ultrashort optical pulses

Zhen Hao, Biqiang Jiang ,[*] Yuxin Ma, Ruixuan Yi, Xuetao Gan,[†] and Jianlin Zhao

Key Laboratory of Light Field Manipulation and Information Acquisition, Ministry of Industry and Information Technology, and Shaanxi Key Laboratory of Optical Information Technology, School of Physical Science and Technology, Northwestern Polytechnical University, Xi'an, 710129, People's Republic of China

Recent advances in laser technology demand more-effective measurement of ultrashort optical pulses in fiber optics and nanophotonics devices. Here we propose an in-fiber strategy to characterize ultrashort pulses by incorporating a gallium selenide–assisted microfiber, as a frequency-doubling block, in an all-fiber interferometer. Pulses to be retrieved were first split into the two arms of the interferometer and then overlapped, exciting the interferometric autocorrelated second harmonic in the microfiber due to high second-order nonlinearity of gallium selenide. In the experiment, the autocorrelator shows high accuracy in measuring 7.13-ps, 1239-fs, and 683-fs pulses. In comparison with a commercial frequency-resolved optical gating, the relative errors are only 1.53%, 3.74%, and 6.86%, respectively. Moreover, by attenuation of the incident laser of one arm of the interferometer, the measured peak-to-background ratio was less than the conventional theoretical value. The proposed autocorrelator could be very compatible with current systems for future applications of in-fiber or on-chip ultrafast optical technology.

I. INTRODUCTION

Ultrashort optical pulses, whose duration in the time domain is on the magnitude of 1 ps or less, have been widely applied in fields ranging from fiber lasers [1–3], structured-light-field generation [4–6], laser processing [7,8], and nonlinear laser microscopy [9,10] to telecommunication [11]. Many techniques have been developed for measuring ultrashort optical pulses in ultrafast optics. With use of a combination of a photodiode and an oscilloscope, direct measurement can be performed readily for pulses of hundreds of picoseconds, where the detectable pulse duration is usually limited by the response time (approximately 10^{-14} s) of the photoelectric effect or the bandwidth of oscilloscopes [12–14]. An electro-optical streak camera is also able to directly characterize pulses with durations of 1 ps or less [15,16]. However, it operates in the visible spectral region, and the increased cost of commercial devices hinders their potential in routine engineering applications [14]. The indirect methods mainly include conventional autocorrelators [17], a frequency-resolved optical gating (FROG) [18,19], and spectral phase interferometry for direct electric field reconstruction [20,21], which

could extend the measurable pulse duration to subpicoseconds. However, because of the built-in bulky second-order nonlinear crystals and elaborate optical and mechanical configurations such as microdisplacement stages, commercial intensity autocorrelators inevitably occupy a large space, which makes them difficult to integrate in some compact fiber or on-chip platforms to characterize ultrashort optical pulses [22–24]. Subsequently developed interferometric autocorrelators further require an accurately calibrated collinear beam geometry [25], which is difficult to realize because there are several very sensitive degrees of freedom in aligning two collinear pulses.

In this work, we report the characterization of ultrashort pulses in an all-fiber autocorrelator assisted by a microfiber. Specifically, by incorporating a gallium selenide (GaSe) crystal–transferred microfiber into a Mach-Zehnder interferometer (MZI), we establish an MZI-microfiber autocorrelator. Then, from the recorded interferometric autocorrelation (AC) curve reflecting the extent of pulse overlapping, the temporal profile and pulse duration of the input pulse can be retrieved. By theoretical calculations, we investigate the dependence of an interferometric AC pattern on typical pulse parameters, including pulse shape, pulse duration, and unequal amplitude ratio of the two MZI arms. In experiments, a C-telecom-band ultrashort pulse train to be measured was incident into the MZI-microfiber autocorrelator. Corresponding experimental

---

*bqjiang@nwpu.edu.cn
†xuetaogan@nwpu.edu.cn

results reveal excellent performance in the measurement of picosecond and femtosecond pulses. Besides, by attenuation of the incident laser of one MZI arm, a peak-to-background ratio (PBR) less than the conventional value of 8 was demonstrated [26]. Therefore, as a building block, the proposed compact MZI-microfiber autocorrelator not only opens up an avenue to conveniently characterize ultrashort optical pulses in fiber or on-chip applications but also expands the usage scope of layered nanomaterials.

II. RESULTS AND DISCUSSION

A. Operation principle of the MZI-microfiber autocorrelator

The experimental system for observing interference spectra with the MZI and measuring the interferometric autocorrelated second harmonic (SH) is sketched in Fig. 1(a) (see Supplemental Material [27] for detailed descriptions). A train of ultrashort laser pulses coupled into the MZI is equally divided into the two optical arms by an optical coupler, and a miniaturized electrically controlled optical delay line is inserted into one of the two arms to create an additional phase delay for the passing pulses. The coherent pulse trains from the two arms then overlap at the output end of the MZI, producing the interferometric autocorrelated SH.

It is necessary to primarily distill the essential physical principle of interferometric AC. The correlation state can be cataloged as three main types, complete uncorrelation, partial correlation, and complete correlation, as schematically illustrated in Fig. 1(b) and Video 1 of the Supplemental Material [27]: (A) Complete uncorrelation means the absolutely separated two ultrashort pulses in the spatial domain. As the background of the AC trace, the excited SH under this condition will have no difference whatever the coherence of the incident laser. (B) Partial correlation indicates the reduced spatial distance and partial overlap of two incident pulses. When overlapped optical cycles within two pulses are in phase, the total incident field is strengthened by constructive interference, and the coherent-SH intensity produced will exceed the incoherent-SH intensity, as marked by yellow rectangles in Fig. 1(b). For the case of antiphased optical cycles within the overlapping part of the two pulses, the total incident field will be weakened due to destructive interference, resulting in a coherent SH weaker than the incoherent SH. (C) Complete correlation signifies the two synchronously propagated pulses, and the corresponding optical cycles in their pulse envelopes are always in phase. Because of total constructive interference, the intensity of the coherent SH will be 8 times that of the incoherent SH, which was theoretically investigated in previous reports [26,28]. By artificially controlling the relative phase difference between two ultrashort pulses, the coherent SH described in states A–C can be experimentally realized.
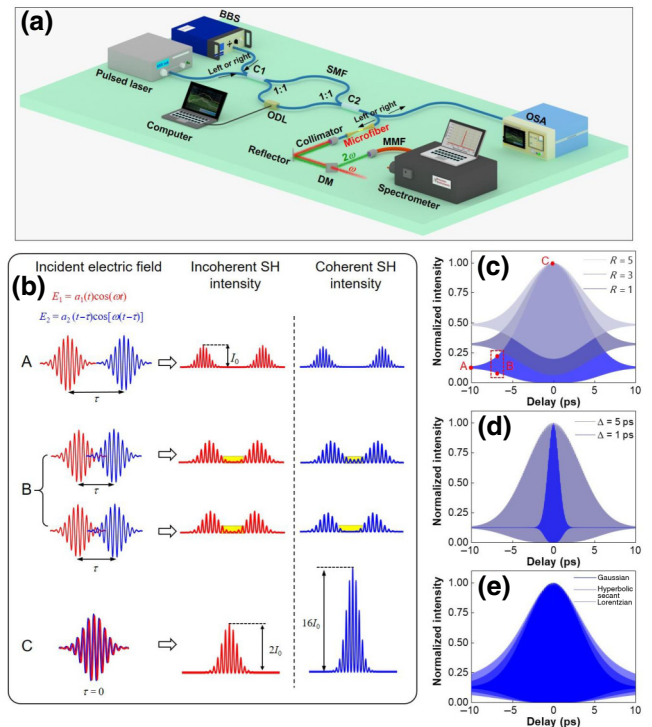

FIG. 1. (a) Experimental setup for observing interference spectra with an MZI and measuring the interferometric autocorrelated SH. (b) Physical principle of the interferometric autocorrelated SH (see Video 1 of the Supplemental Material [27] for a demonstration of two overlapped femtosecond pulses). (c)–(e) Traces of the interferometric autocorrelated SH for different amplitude ratios ($R = 5$, 3, and 1) of two pulses, pulse durations ($\Delta = 5$ ps and 1 ps), and pulse shapes (Gaussian, Lorentzian, and hyperbolic secant). BBS, broadband source; C1, coupler 1; C2, coupler 2; DM, dichroic mirror; MMF, multimode fiber; OSA, optical spectrum analyzer; SMF, single-mode fiber.

The corresponding modulation curve constitutes the AC trace, from which typical pulse parameters such as pulse shape, pulse duration, and amplitude ratio of two pulses may be retrieved.

To further obtain intuitive insight into the dependences of the AC trace on the aforementioned typical pulse parameters, preliminary theoretical calculations were performed. With two pulses expressed as $E_1 = a_1(t)\cos(\omega t)$ and $E_2 = a_2(t - \tau)\cos[\omega(t - \tau)]$ in the time domain, the amplitude ratio of the two pulses is well defined as $R = \max[a_1(t)]/\max[a_2(t)]$, where $a_1(t)$ and $a_2(t)$ express the pulse envelopes and τ is the time delay between the two pulses. For a fixed pulse duration of 5 ps, Fig. 1(c) gives AC traces when R is 1, 3, and 5, wherein the SH intensities have been normalized to their maximums. The standard AC trace corresponds to the case of $R = 1$, where the red points A, B, and C in Fig. 1(c) indicate the three types of correlation state mentioned earlier. Points C and A illustrate the completely correlated peak SH and

completely uncorrelated background SH, and the intensity ratio between them (PBR) has been demonstrated as being 8:1 [26,28]. As shown in the two faint-blue AC traces in Fig. 1(c), with the increasing of R, the PBR will decrease accordingly. The theoretical lower limiting value of the PBR is 1, describing the circumstance that one weak pulse is almost overwhelmed by the other, distinctly stronger pulse. We also investigated the evolution of the autocorrelated SH with changed pulse duration Δ, and the calculation represented in Fig. 1(d) reveals a narrower full width at half maximum (FWHM) of the AC trace for a 1-ps pulse. The calculations represented in Figs. 1(c) and 1(d) were done on the premise that a Gaussian pulse is incident. However, as laser sources of other kinds may be used in practical applications, interferometric AC traces for Lorentzian and hyperbolic secant pulses are also shown in Fig. 1(e). With the same pulse duration as for the aforementioned Gaussian pulse, the 5-ps Lorentzian or hyperbolic secant pulse leads to a slightly wider FWHM of the AC trace, which is ascribed to a flatter front and tail of Lorentzian and hyperbolic secant–shaped pulse envelopes. The basic principles sketched in Figs. 1(b)–1(e) work in any kind of second-order interferometric autocorrelator using second-order frequency up-conversions.

B. Peparation of the microfiber frequency-doubling element

Taking into account the miniaturization of the experimental system and the ultrahigh nonlinearity of GaSe, we used a GaSe-transferred microfiber as the frequency-doubling element, as sketched in Fig. 2(a). In the fabrication, a pristine microfiber was first drawn from a single-mode fiber by the flame-brushing technique, with a taper-waist diameter of 3.5 μm [Fig. 2(b)], which is close to the theoretical phase-matching diameter of the $EH_{11}(2\omega)$ and $HE_{31}(2\omega)$ modes [29]. There is another phase-matching diameter of approximately 0.8 μm for the $HE_{11}(\omega)$ and $HE_{21}(2\omega)$ modes [30]; however, this diameter was not selected due to the difficulty in transferring layered GaSe onto such a thin microfiber. Then, with the dry-transfer technique, a thin-layered GaSe crystal (mechanically exfoliated from a bulk GaSe crystal) was transferred onto the tapered region to establish the GaSe-transferred microfiber (see Supplemental Material [27] for details). Bright-field and dark-field images of the microfiber are shown in Fig. 2(b), and the red light was attributed to scattering of the GaSe coating wrapped on the microfiber surface. Finally, we measured transmission spectra of the GaSe-transferred microfiber around the pump and SH wavelengths. As shown in Fig. 2(c), the losses of 2–4 dB demonstrate excellent device performance of the GaSe-transferred microfiber and lay sufficient foundation for subsequent interferometric AC experiments, in which a strong SH signal is desired.

Moreover, we discuss some experimental factors that can affect the intensity and signal-to-noise ratio of the SH signal, which is related to the accuracy of the characterization results for ultrashort optical pulses. The intensity of the output total SH is affected by various factors, including the diameter of the microfiber [29–31], the temperature of the experimental environment, the length of the GaSe coating, and the polarization direction of the pump laser [32]. These factors are related to different physical parameters in Eq. (2), such as the phase-mismatch parameter $\Delta\beta_{SH}$, the nonlinear interaction length L, and the nonlinear coupling parameter κ. Specifically, the phase-mismatch parameter $\Delta\beta_{SH}$ is a critical factor that affects the intensity of the SH signal and is positively correlated with an increase in the microfiber diameter or the perturbation of the surrounding temperature, resulting in a smaller SH intensity. However, in this work, the contribution of this factor may not be dominant because the absolute value of $\Delta\beta_{SH}L/2$ remains small. This is attributed to the micron-level length L of the GaSe coating, which reduces the impact of the phase-mismatch parameter on the SH intensity. The nonlinear coupling parameter κ is sensitive to the polarization direction of the pump laser, particularly when the equivalent coverage ratio of the GaSe coating is low [32]. Therefore, careful control of the polarization direction of the pump laser is essential to achieve sufficient SH intensity in microfibers with low-coverage GaSe coatings.
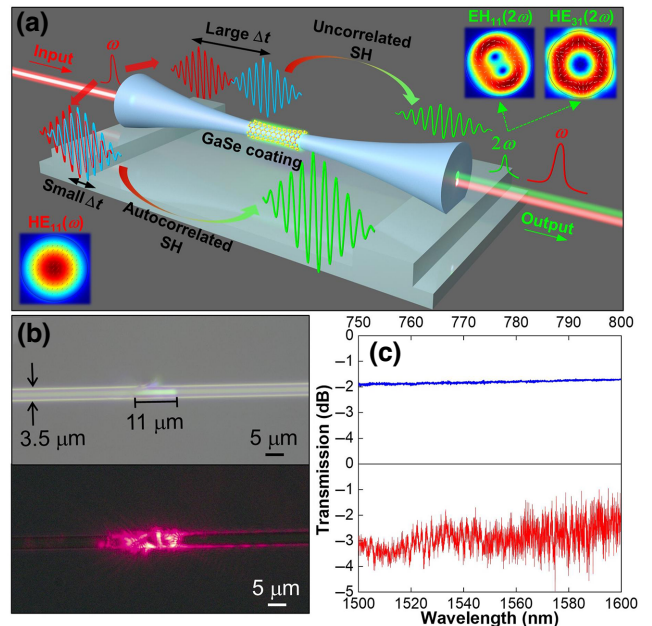

FIG. 2.   (a) A GaSe-transferred microfiber as a platform for enhancement of SH intensity, with phase-matched mode profiles shown in the insets. (b) Optical microscope images of the GaSe-transferred microfiber under bright and dark fields. (c) Transmission spectra of the GaSe-transferred microfiber around pump and SH wavelengths.

C. Characterization results for ultrashort optical pulses

When an ultrashort pulse train is incident into the MZI-microfiber autocorrelator and divided into the two arms, considering the introduced phase delay and accumulated SH from different axial positions of the microfiber, the intensity of the output signal ($I_{2\omega}$) is determined by [26,28,30,32–34]

$$I_{2\omega}(\tau) = I_0 V(\tau), \tag{1}$$

$$I_0 = |\kappa|^2 L^2 \mathrm{sinc}^2\left(\frac{\Delta\beta_{\mathrm{SH}}L}{2}\right), \tag{2}$$

$$V(\tau) = \int_{-\infty}^{\infty} |a_1(t)\cos(\omega t) + a_2(t-\tau)\cos[\omega(t-\tau)]|^4 dt, \tag{3}$$

where the excited total SH is formally expressed in Eq. (1), which is collectively determined by the phase-matching condition and AC described in Eqs. (2) and (3), respectively. In Eq. (2), L is the nonlinear interaction length and $\Delta\beta_{\mathrm{SH}} = 2\beta_\omega - \beta_{2\omega}$ is the phase-mismatch parameter between the pump and signal modes, where β_ω and $\beta_{2\omega}$ are the respective propagation constants. It can be found from Eq. (2) that a near-zero $\Delta\beta_{\mathrm{SH}}$ is conducive to the creation of a strong SH, which can be guaranteed by controlling the microfiber diameter to engineer the waveguide dispersion in the fabrication process [30]. In this case, the phase-matching condition is satisfied, meaning synchronously propagated wave fronts of the SH and pump light in the spatial domain and a 2 times increased phase of the SH in contrast to the pump. The nonlinear coupling parameter $\kappa \propto \int \mathbf{P}_{2\omega} \cdot \mathbf{e}_{2\omega} dS$ is determined by the coupling of second-order nonlinear polarization to the $\mathrm{EH}_{11}(2\omega)$ and $\mathrm{HE}_{31}(2\omega)$ modes, in which $\mathbf{e}_{2\omega}$ expresses the normalized electric field of the SH mode and the integration is performed in the infinite plane perpendicular to the longitudinal direction of the microfiber [32,35]. In Eq. (3), $a_1(t)$ and $a_2(t)$ express corresponding amplitude envelopes of the two divided pulses and τ is the relative time delay between them. The high-frequency oscillated optical cycles under the two pulse envelopes are described by two cosine functions in Eq. (3), and it is the two functions that are responsible for the quite-dense oscillations in the interferometric AC trace. $V(\tau)$ depends on the fourth power of the right-hand side of Eq. (3) [32,36], which originates from the more-fundamental relationship between the SH intensity and the pump field amplitude ($I_{2\omega} \propto |E_\omega|^4$). Note that the integration in Eq. (3) is performed over the whole time domain (from $-\infty$ to $+\infty$) to contain all optical cycles under the two interfering pulses.

To experimentally demonstrate the physical principle of standard AC and the feasibility of the MZI-microfiber autocorrelator, a 1550-nm picosecond-pulse laser with a pulse duration of 7.13 ps and a repetition rate of 18.5 MHz was incident into the experimental setup shown in Fig. 1(a). With the time delay of the electrically controlled optical delay line increased in fixed intervals of 0.06 ps, we measured the corresponding interferometric autocorrelated SH under approximately 4.5-mW pump power in a room without air flow. As shown in Fig. 3(a), the area occupied by the many blue data points constitutes a bell-shaped AC trace; the PBR almost equals 8, and dramatic oscillations and the existence of the lower envelope collectively confirm the nature of second-order interferometric AC [26]. To retrieve typical parameters of the incident pulse, some theoretical calculations were subsequently performed, in which the pulse was assumed to be Gaussian shaped with slowly varying amplitudes of the two arms' pulses described by $a_1(t) = e^{-(1+iC)t^2/(2t_0^2)}$ and $a_2(t-\tau) = e^{-(1+iC)(t-\tau)^2/(2t_0^2)}$, where C is the chirp parameter, t_0 denotes the duration at $1/e$ intensity, and FWHM is $2\sqrt{\ln 2}$ (approximately 1.665) times that of t_0 [14]. According to Eq. (3), the theoretical interferometric AC trace is obtained, represented by the solid gray line in Fig. 3(a). Its upper and lower envelopes, represented by dashed black lines, are proportional to $\int |a_1(t) \pm a_2(t-\tau)|^4 d\tau$, where plus and minus signs correspond to the upper envelope and the lower envelope, respectively [26,28]. By optimization of the values of t_0 and C to make the trend reflected by the blue data points well contained by the upper and lower envelopes, a 7.24-ps duration of the incident pulse is retrieved, with C equaling 1.2.
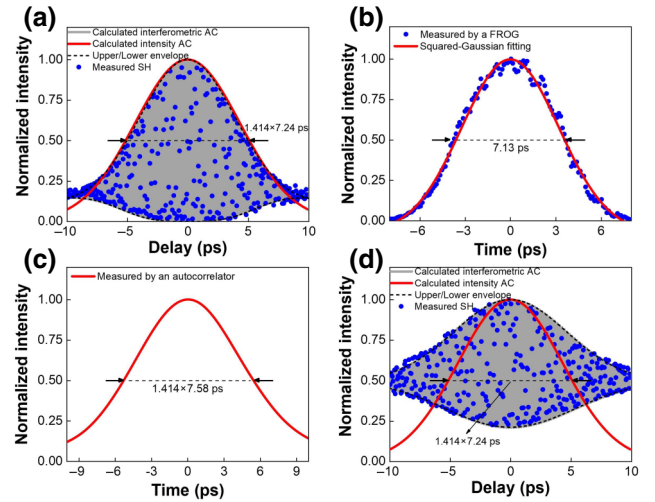

FIG. 3. Autocorrelated SH excited by a light source with a Gaussian pulse. (a) Interferometric AC trace for a Gaussian pulse train, with its duration obtained as 7.24 ps. (b) Temporal profile of the 7.13-ps Gaussian pulse used for (a), characterized by a commercial FROG. (c) Intensity AC trace of the Gaussian pulse used, characterized by a commercial autocorrelator. (d) Evolved trace from (a) when the amplitude ratio R is changed to around 5.

Described by $A(\tau) = \int_{-\infty}^{+\infty} I_1(t)I_2(t-\tau)dt$ [37], the intensity AC trace with the above-mentioned pulse parameters is indicated by the solid red line in Fig. 3(a), where $I_1(t)$ and $I_2(t-\tau)$ express the optical intensities in two MZI arms, respectively. Characterized by a commercial FROG, from Fig. 3(b), the incident pulse was found to be Gaussian shaped with a duration of 7.13 ps. This is similar to the 7.58-ps duration characterized by a commercial autocorrelator in Fig. 3(c), in which the deconvolution factor of $\sqrt{2} \approx 1.414$ gives the ratio of the full widths at half maximum between the intensity AC trace and the corresponding pulse duration for a Gaussian pulse [37,38]. The intensity AC trace is described by $A(\tau) = \sqrt{(\pi/2)}t_0 e^{-\frac{1}{2}\tau^2/t_0^2}$. The slight deviations of 1.54% and 4.49% reveal the favorable basic operation performance of the MZI-microfiber autocorrelator for characterizing picosecond pulses. Additionally, to obtain further insight, we discuss the relationship between interferometric and intensity AC traces. The minimum value of $A(\tau)$ appearing at delay $\tau = \pm 10$ ps corresponds to the almost-completely-uncorrelated background SH in the interferometric AC trace. When the MZI was adjusted to a closely balanced state with a nearly infinite free spectral range as illustrated in Fig. S1(b) in Supplemental Material [27], $A(\tau)$ increases to the maximum at exactly $\tau = 0$ ps, indicating complete correlation of the two pulse trains and thus a maximized interferometric autocorrelated SH. However, at the next delay increment or decrement of half an optical cycle (quite close to 0 ps), the two pulses add with opposite phase, resulting in a near-zero signal.

By changing the amplitude ratio of the two arms' pulses, we also invesigated a nonstandard interferometric AC trace ($R \neq 1$, PBR not equal to 8). In the experiment, using the same experimental arrangement as for standard interferometric AC in Fig. 3(a) but attenuating the carried power by virtually connecting one MZI arm's fiber patch cord, we tuned the amplitude ratio R of the two arms to 5. Differently from standard interferometric AC, the trace in Fig. 3(d) has a flatter bell shape, corresponding to a PBR of 2, which is smaller than the conventional value of 8. A distinct difference between Figs. 3(a) and 3(d) is the nonzero SH minimum near $\tau = 0$ ps. This is induced by the two unbalanced MZI arms, leading to the incomplete destructive interference of the two pulse trains. The gray theoretical interferometric AC trace in Fig. 3(d) is calculated for a 7.24-ps duration of the incident Gaussian pulse, which is in accordance with the retrieved pulse duration shown in Fig. 3(a).

The MZI-microfiber autocorrelator has a wide measurable applicability with regard to pulse shape and pulse duration, which could be extended to a femtosecond Lorentzian pulse. As shown in Fig. 4(a), with the previously used 7.13-ps Gaussian pulse replaced by a 1239-fs Lorentzian pulse, the AC trace is significantly narrowed

in comparison with the AC trace in Fig. 3(a). This is reasonable because of the 5.8 times reduced pulse duration. To obtain the theoretical trace and retrieve its pulse duration, we assumed there are Lorentzian pulse envelopes in the two MZI arms and mathematically described them by $a_1(t) = 1/(t_1^2 + t^2)$ and $a_2(t - \tau) = 1/[t_1^2 + (t - \tau)^2]$ [39], where the FWHM of the pulse duration is $2\sqrt{\sqrt{2}-1}$ (approximately 1.287) times that of t_1. According to Eq. (3) and the optimized parameter t_1, the theoretical interferometric AC trace was calculated, and the corresponding duration of the incident pulse was obtained as 1287 fs. Measured by the commercial FROG, in Fig. 4(b), the incident pulse was identified as Lorentzian shaped with a duration of 1239 fs, which indicates a relative error of 3.87% for the proposed autocorrelator. This is in accordance with measurement results for 1332 fs obtained with a previously used commercial autocorrelator in Fig. 4(c) (the deconvolution factor of 1.654 gives the ratio of the full widths at half maximum between
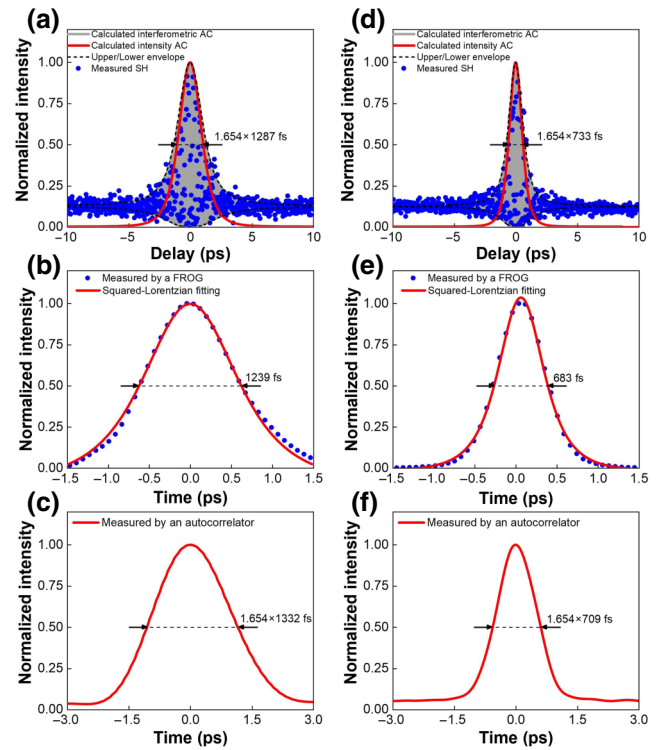

FIG. 4. Autocorrelated SH excited by light sources with different pulse parameters. (a) Interferometric AC trace for a Lorentzian pulse train with a duration of 1239 fs. (b),(c) Temporal profile and intensity AC trace of the Lorentzian pulse used for (a), characterized by a commercial FROG and a commercial autocorrelator, respectively. (d) Interferometric AC trace for another, narrower Lorentzian pulse with a duration of 683 fs. (e),(f) Temporal profile and intensity AC trace of the Lorentzian pulse used for (d), characterized by a commercial FROG and a commercial autocorrelator, respectively.

the intensity AC trace and the corresponding pulse duration for a Lorentzian pulse, where the intensity AC trace is described by $A(\tau) = \pi(\tau^2 + 20t_1^2)/[t_1^3(\tau^2 + 4t_1^2)^3])$ and the corresponding relative error is 3.38%. Further, we replaced the incident laser with another Lorentzian pulse with a shorter pulse duration of hundreds of femtoseconds, and a similar interferometric AC trace but with a narrower FWHM was recorded. According to Fig. 4(d), a duration of 733 fs was obtained. The corresponding relative errors are 7.32% and 3.39% compared with the characterization results obtained with the commercial FROG (683 fs) and the commercial autocorrelator (709 fs), as shown in Figs. 4(e) and 4(f). As another reflection of the aforementioned relative errors, the experimental PBRs from Figs. 4(a) and 4(d) decrease to 7.3 and 7.0, which are slightly smaller than the theoretical value of 8. This may be ascribed to possible vibration, air disturbance of the surrounding environment, and voltage instability. These factors could additionally introduce an undesired phase difference into the two MZI arms and therefore change the SH intensity, whose harmful effect is more detectable for ultrashort pulses.

D. Calibration of pulse characterization results

To calibrate the measured pulse duration, we investigated the broadening of incidence pulses induced by the waveguide dispersion of the microfiber. First, by the finite-element method, we simulated the wavelength-dependent effective refractive index (n_{eff}) of the $HE_{11}(\omega)$ mode for a given diameter D. Then, through the sequential use of $n_g = n_{\text{eff}} - \lambda dn_{\text{eff}}/d\lambda$ and $D_w = (1/c)dn_g/d\lambda$, the waveguide dispersion D_w for the given diameter D can be calculated, where n_g and c mean the group refractive index and the speed of light in a vacuum, respectively [40,41]. Finally, by changing the diameter D, we obtained the evolution of the waveguide dispersion D_w with the microfiber diameter. As illustrated in Fig. 5(a), the waveguide dispersion increases dramatically from near zero to 103 ps/nm km at a wavelength of 1550 nm when the fiber diameter is decreased from 125 to 3.5 μm. The incident pulse constantly broadened when it propagated from the transition region (approximately 80 mm) to the middle point of the uniform tapered region (approximately 5 mm), where the GaSe coating was transferred. The total pulse-duration broadening can be calculated by integration of the waveguide dispersion over the faint-red area in Fig. 5(b) and then multiplication by the spectral width of the laser [40]. The spectral width of the laser used for Figs. 3(a), 3(d) is 0.5 nm, while spectral widths of the lasers used for Figs. 4(a), 4(d) are 0.93 and 1.7 nm, respectively, implying broadening of 0.93-fs for the AC experiments in Figs. 3(a) and 3(d) while 1.72 and 3.15-fs for Figs. 4(a) and 4(d). According to the calculated results, the relative errors of the measurement results for the Gaussian and Lorentzian pulses in Figs. 3 and 4 were corrected to
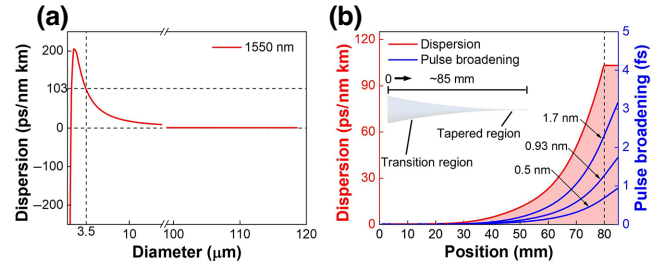
FIG. 5. (a) Calculated waveguide dispersion when a pulse centered at 1550 nm is used. (b) Corresponding pulse broadening versus microfiber position.

1.53%, 3.74%, and 6.86% in comparison with the commercial FROG and 4.50%, 3.51%, and 2.94% in comparison with the commercial autocorrelator.

III. CONCLUSION

In summary, we propose an alignment-free microfiber interferometric autocorrelator for the characterization of ultrashort pulses, with broad measurement applicability for picosecond and femtosecond pulses. The compact GaSe-transferred microfiber, as a cost-effective and readily integrated frequency-doubling element compared with conventional bulky crystals or fiber-coupled-waveguide nonlinear crystals such as periodically poled lithium niobate, was incorporated into an MZI to establish the autocorrelator [29,42]. For a picosecond Gaussian pulse in the C telecom band, typical pulse parameters, including shape and duration, were accurately retrieved from its AC trace, and a nonstandard AC trace with a PBR of 5 was experimentally demonstrated by attenuation of the light power carried by one of the MZI arms. As expected, by our further replacing the incident laser with femtosecond pulses, the applicability of the MZI-microfiber autocorrelator was extended. Moreover, because of various factors, such as the diameter of the microfiber and the length and thickness of the GaSe coating, the phase-matching bandwidth of the proposed autocorrelator may vary within a limited range. Nevertheless, it is possible to artificially control the phase-matching wavelength by engineering the microfiber diameter, which in principle allows the fabrication of autocorrelators operating from the visible to the infrared spectral region. We believe the advantages such as compact size, high sensitivity, and broad operation range with regard to pulse duration offer insights into improving interferometric autocorrelators with a collinear configuration, which makes the proposed alignment-free microfiber autocorrelator an attractive alternative for characterization of ultrashort optical pulses in all-fiber or on-chip applications.

ACKNOWLEDGMENTS

---

[1] N. Nishizawa, Generation of optical harmonics, Jpn. J. Appl. Phys. **53**, 090101 (2014).

[2] H. Zhang, Y. Zheng, D. Mao, C. Zeng, Y. Du, and J. Zhao, Morphology-controllable ultrafast fiber lasers based on intracavity manipulation of transverse modes, Phys. Rev. Appl. **16**, 034045 (2021).

[3] D. Mao, Q. Gao, J. Li, Z. He, Y. Du, C. Zeng, Z. Sun, and J. Zhao, Birefringence-induced heterogeneous vector pulses in ultrafast fiber lasers, Phys. Rev. Appl. **18**, 044044 (2022).

[4] D. Mao, Y. Zheng, C. Zeng, H. Lu, C. Wang, H. Zhang, W. Zhang, T. Mei, and J. Zhao, Generation of polarization and phase singular beams in fibers and fiber lasers, Adv. Photon. **3**, 014002 (2021).

[5] A. Forbes, Structured light from lasers, Laser Photon. Rev. **13**, 1900140 (2019).

[6] N. Rana, M. S. Mrudul, and G. Dixit, Generation of circularly polarized high harmonics with identical helicity in two-dimensional materials, Phys. Rev. Appl. **18**, 064049 (2022).

[7] M. Malinauskas, A. Žukauskas, S. Hasegawa, Y. H. V. Mizeikis, R. Buividas, and S. Juodkazis, Ultrafast laser processing of materials: from science to industry, Light Sci. Appl. **5**, e16133 (2016).

[8] K. Sugioka, Progress in ultrafast laser processing and future prospects, Nanophotonics **6**, 393 (2017).

[9] Y. Ozeki, W. Umemura, Y. Otsuka, S. Satoh, H. Hashimoto, K. Sumimura, N. Nishizawa, K. Fukui, and K. Itoh, High-speed molecular spectral imaging of tissue with stimulated Raman scattering, Nat. Photon. **6**, 845 (2012).

[10] N. Zhou, A. Zheng, K. K. Y. Wong, and R. Zhou, High-resolution quantitative phase microscopy with second-harmonic generation and structured illumination from a k-space formulation, Phys. Rev. Appl. **18**, 054028 (2022).

[11] W. H. Knox, Ultrafast technology in telecommunications, IEEE J. Sel. Top. Quantum Electron. **6**, 1273 (2000).

[12] D. J. Bradley and G. H. C. New, Ultrashort pulse measurements, Proc. IEEE **62**, 313 (1974).

[13] C. H. Lin and T. K. Gustafson, Optical pulsewidth measurement using self-phase modulation, IEEE J. Quantum Electron. **8**, 429 (1972).

[14] G. P. Agrawal, *Nonlinear Fiber Optics* (Elsevier, New York, 2019), 6th ed.

[15] D. J. Bradley, B. Liddy, and W. E. Sleat, Direct linear measurement of ultrashort light pulses with a picosecond streak camera, Opt. Commun. **2**, 391 (1971).

[16] A. Takahashi, M. Nishizawa, Y. Inagaki, M. Koishi, and K. Kinoshita, New femtosecond streak camera with temporal resolution of 180 fs, Proc. SPIE **2116**, 275 (1994).

[17] H. P. Weber, Method for pulsewidth measurement of ultrashort light pulses generated by phase-locked lasers using nonlinear optics, J. Appl. Phys. **38**, 2231 (1967).

[18] R. Trebino, K. W. DeLong, D. N. Fittinghoff, J. N. Sweetser, M. A. Krumbugel, and B. A. Richman, Measuring ultrashort laser pulses in the time-frequency domain using frequency-resolved optical gating, Rev. Sci. Instrum. **68**, 3277 (1997).

[19] D. J. Kane and R. Trebino, Characterization of arbitrary femtosecond pulses using frequency-resolved optical gating-resolved optical gating, IEEE J. Quantum Electron. **29**, 571 (1993).

[20] C. Iaconis and I. A. Walmsley, Spectral phase interferometry for direct electric-field reconstruction, Opt. Lett. **23**, 792 (1998).

[21] Y. Mairesse, O. Gobert, P. Breger, H. Merdji, P. Meynadier, P. Monchicourt, M. Perdrix, P. Salieres, and B. Carre, High harmonic XUV spectral phase interferometry for direct electric-field reconstruction, Phys. Rev. Lett. **94**, 173903 (2005).

[22] X. Guo, C. Zou, C. Schuck, R. C. Hojoong Jung, and H. X. Tang, Parametric down-conversion photon-pair source on a nanophotonic chip, Light Sci. Appl. **6**, e16249 (2017).

[23] B. Wang, Y. Ji, L. Gu, L. Fang, X. Gan, and J. Zhao, High-efficiency second-harmonic and sum-frequency generation in a silicon nitride microring integrated with few-layer GaSe, ACS Photon. **9**, 1671 (2022).

[24] S. Richard, Second-harmonic generation in tapered optical fibers, Opt. Lett. **27**, 1504 (2010).

[25] K. Naganuma, K. Mogi, and H. Yamada, General method for ultrashort light pulse chirp measurement, IEEE J. Quantum Electron. **25**, 1225 (1989).

[26] D. Meshulach, Y. Barad, and Y. Silberberg, Measurement of ultrashort optical pulses by third-harmonic generation, J. Opt. Soc. Am. B **14**, 2122 (1997).

[27] See Supplemental Material at http://link.aps.org/supplemental/10.1103/PhysRevApplied.20.044023 for detailed descriptions on the experimental setup used and the fabrication process for the GaSe-transferred microfiber and a video demonstrating the correlation state of two femtosecond pulses.

[28] J.-C. M. Diels, J. J. Fontaine, I. C. McMichael, and F. Simoni, Control and measurement of ultrashort pulse shapes (in amplitude and phase) with femtosecond accuracy, Appl. Opt. **24**, 1270 (1985).

[29] B. Jiang, Z. Hao, Y. Ji, Yueguo Hou, R. Yi, Dong Mao, Xuetao Gan, and J. Zhao, High-efficiency second-order nonlinear processes in an optical microfibre assisted by few-layer GaSe, Light Sci. Appl. **9**, 63 (2020).

[30] J. Chen, J. Tan, G. Wu, X. Zhang, F. Xu, and Y. Lu, Tunable and enhanced light emission in hybrid WS_2-optical-fiber-nanowire structures, Light Sci. Appl. **8**, 8 (2019).

[31] Z. Hao, B. Jiang, Y. Ma, R. Yi, H. Jin, L. Huang, X. Gan, and J. Zhao, Strain-controlled phase matching of optical harmonic generation in microfibers, Phys. Rev. Appl. **19**, L031002 (2023).

[32] Z. Hao, B. Jiang, Y. Hou, C. Li, R. Yi, Y. Ji, J. Li, A. Li, X. Gan, and J. Zhao, Continuous-wave pumped frequency upconversions in an InSe-integrated microfiber, Opt. Lett. **46**, 733 (2021).

[33] J. Lægsgaard, Theory of surface second-harmonic generation in silica nanowires, J. Opt. Soc. Am. B **27**, 1317 (2010).

[34] Z. Hao, Y. Ma, B. Jiang, Y. Hou, A. Li, R. Yi, X. Gan, and J. Zhao, Second harmonic generation in a hollow-core

fiber filled with GaSe nanosheets, Sci. China Inf. Sci. **65,** 162403:1 (2022).

[35] C. Ciret, K. Alexander, N. PoulvellariEe, M. Billet, C. M. Arabi, B. Kuyken, S.-P. Gorza, and F. Leo, Influence of longitudinal mode components on second harmonic generation in III-V-on-insulator nanowires, Opt. Express **28,** 31584 (2020).

[36] R. W. Boyd, *Nonlinear Optics* (Elsevier, Singapore, 2010), 3rd ed.

[37] A. M. Weiner, *Ultrafast Optics* (John Wiley & Sons, New Jersey, 2009), 1st ed.

[38] Y. Zhu, C. Zeng, Z. He, Q. Gao, H. Wang, Y. Du, and D. Mao, Ultrafast all-anomalous-dispersion Er-doped large-mode-area fiber lasers, Opt. Laser Technol. **148,** 107783 (2020).

[39] L. M. Frantz and J. S. Nodvik, Theory of pulse propagation in a laser amplifier, J. Appl. Phys. **34,** 2346 (1963).

[40] Z. Shi, J. Zhang, L. Yang, H. Wu, N. Yao, J. Gong, W. Fang, P. Wang, X. Guo, and L. Tong, Miniature optical correla-tor in a single-nanowire Sagnac loop, ACS Photon. **7,** 3264 (2020).

[41] L. Tong, J. Lou, and E. Mazur, Single-mode guiding properties of subwavelength-diameter silica and silicon wire waveguides, Opt. Express **12,** 1025 (2004).

[42] D. D. Hickstein, D. R. Carlson, A. Kowligy, M. Kirchner, S. R. Domingue, N. Nader, H. Timmers, A. Lind, G. G. Ycas, M. M. Murnane, H. C. Kapteyn, S. B. Papp, and S. A. Diddams, High-harmonic generation in periodically poled waveguides, Optica **4,** 1538 (2017).

Correction: An error in the proof production cycle resulted in Video 1 of the Supplemental Material (SM) being presented as part of the main paper, with static images and a caption. The images and caption have been removed; all citations of the video in text now point to the SM reference. The SM reference itself has been adjusted to include a description of the video.